applied optics

Transformable Reflective Telescope for optical testing and education

Woojin Park,[1,6] Soojong Pak,[1,*] Geon Hee Kim,[2] Sunwoo Lee,[1] Seunghyuk Chang,[3] Sanghyuk Kim,[4] Byeongjoon Jeong,[2] Trenton James Brendel,[5] and Dae Wook Kim[5]

[1]School of Space Research and Institute of Natural Science, Kyung Hee University, Yongin 17104, South Korea
[2]Korea Basic Science Institute, 169-148, Daejeon 34133, South Korea
[3]Center for Integrated Smart Sensors, Korea Advanced Institute of Science and Technology (KAIST), Daejeon 34141, South Korea
[4]Korea Astronomy and Space Science Institute, Daejeon 34055, South Korea
[5]James C. Wyant College of Optical Sciences, University of Arizona, Tucson, Arizona 85721, USA
[6]e-mail: woojinpark@khu.ac.kr
*Corresponding author: soojong@khu.ac.kr

Received 12 March 2020; revised 19 May 2020; accepted 19 May 2020; posted 19 May 2020 (Doc. ID 392304); published 17 June 2020

We propose and experimentally demonstrate the Transformable Reflective Telescope (TRT) kit for educational purposes and for performing various optical tests with a single kit. The TRT kit is a portable optical bench setup suitable for interferometry, spectroscopy, measuring stray light, and developing adaptive optics, among other uses. Supplementary modules may be integrated easily due to the modular design of the TRT kit. The kit consists of five units: a primary mirror module, secondary mirror module, mounting base module, baffle module, and alignment module. Precise alignment and focusing are achieved using a precision optical rail on the alignment module. The TRT kit transforms into three telescope configurations: Newtonian, Cassegrain, and Gregorian. Students change telescope configurations by exchanging the secondary mirror. The portable design and the aluminum primary mirror of the TRT kit enable students to perform experiments in various environments. The minimized baffle design utilizes commercial telescope tubes, allowing users to look directly into the optical system while suppressing stray light down to $\sim 10^{-8}$ point source transmittance. The TRT kit was tested using a point source and field images. Point source measurement of the Newtonian telescope configuration resulted in an 80% encircled energy diameter of 23.8 μm.

https://doi.org/10.1364/AO.392304

1. INTRODUCTION

Reflective telescopes are based primarily on Newtonian, Cassegrain, and Gregorian designs. The Newtonian optical design is the simplest of the three and is generally well adapted for commercial telescopes. Optical antennas and reflective objective mirrors use modified Cassegrain or Gregorian optical systems [1,2]. Recently, Gregorian designs have become more important in large-aperture telescopes, as the Gregorian secondary mirror can be optically conjugated to the upper layer of the Earth's atmosphere enabling the use of adaptive optics (AO) techniques for diffraction-limited observation [3]. For example, the aplanatic Gregorian optical design of the Giant Magellan Telescope (GMT) utilizes seven segmented primary mirrors, each 8.4 m in diameter, and adaptive secondary mirrors [4].

Newtonian, Cassegrain, and Gregorian optical systems rely chiefly upon a primary mirror and a secondary mirror. The parabolic primary mirror is used to correct for spherical aberration and is common across all three telescope designs. The principal differentiating factors among these three optical designs are the location and surface shape of the secondary mirror. The Transformable Reflective Telescope (TRT) may be reconfigured to each of the optical designs by simply changing the secondary mirror.

A few transformable kits have been introduced that are exchangeable for Newtonian or Cassegrain design. One setup uses a 45° folding mirror within a Cassegrain design to change the setup into a Newtonian telescope [5]. In this kit, the Newtonian setup requires a folding mirror that is larger in size than the secondary mirror found in the Cassegrain design. The other kit places the secondary mirror along the optical axis of the primary mirror. By sliding the convex hyperbolic secondary mirror along the optical axis to the primary mirror, the Cassegrain design is converted to a Newtonian telescope [6]. There is also a method that includes two-optical systems within a single setup by installing the Newtonian and Cassegrain secondary mirrors on a rotatable mount [7]. The Gregorian configuration, however, utilizes a much longer focal length than

the other designs, making it technically difficult to implement all configurations in a single setup.

The transformable optical system also requires optical alignment and baffling to suppress stray light. This necessitates the use of an alignment module, baffles, and optomechanical structures. We present a flexible astronomy educational kit that can be configured into each of the previously described reflective telescopes.

Optical design of the transformable optical system is discussed in Sections 2.A and 2.B. Optomechanical design and structural analysis results are presented in Section 2.C. The fabrication process and mirror surface quality are explored in Section 3.A. Section 3.C describes the optical alignment procedure for this system. Stray light consideration and baffle design are examined in Section 4. Section 5 presents optical performance measurements of the TRT kit. Finally, all the results and possible applications are summarized in Section 6.

2. TRT SYSTEM DESIGN AND ANALYSIS

A. Flexible TRT Optical Design

The TRT kit transforms into three traditional two-mirror optical systems: the Newtonian, Cassegrain, and Gregorian telescopes. Figure 1 illustrates the telescope configurations. In each case, incident rays are reflected from the paraboloidal primary mirror and the secondary mirror sequentially, so that rays converge to a single focal point as depicted in the figure. The Newtonian, Cassegrain, and Gregorian systems use flat, convex hyperboloidal, and concave ellipsoidal secondary mirrors, respectively. The optical design parameters of the primary and secondary mirrors used for the TRT kit are summarized in Table 1.

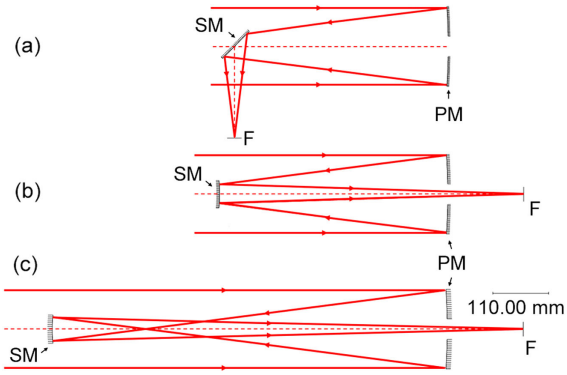

Fig. 1. Optical layout of (a) Newtonian, (b) Cassegrain, and (c) Gregorian telescopes. PM, primary mirror; SM, secondary mirror; F, focal point.

All secondary mirrors have a 50 mm clear aperture. The radius of curvature of the Cassegrain and Gregorian secondary mirrors are −400 mm and +300 mm, respectively. The axial distance between the primary and secondary mirrors, which is also called despace, are 450 mm for Newtonian and Cassegrain, and 778.9 mm for Gregorian. The back focal length of Newtonian, Cassegrain, and Gregorian are 178.5 mm, 600 mm, and 928.9 mm, respectively. The conic constants for the TRT kit Cassegrain and Gregorian configurations are −2.778 and −0.458, respectively. It is worth to note that optimal conic constants for the primary and secondary mirrors can be selected to desensitize the telescope decentration tolerance for two-mirror systems [8]. For the TRT kit, however, a parabolic primary mirror is required for the Newtonian configuration, and such a conic constant optimization is not available.

In the proposed TRT kit, three optical systems share a single primary mirror. Reconfiguring the telescope system requires a simple exchange of the secondary mirror, while the rest of the optomechanical parts remain fixed.

B. Tolerance Analysis

Optical performance changes from assembly and alignment errors are expected based on tolerance analysis. We used CODE V and ZEMAX for sensitivity analysis and Monte Carlo simulation, respectively. Figure 2 shows the coordinate system for tolerance analysis.

Sensitivity analysis is completed to gauge optical performance degradation by optical alignment errors and mechanical deformations. Surface α-, β-, and γ-tilts, x- and y-decentration of each mirror, and despace are examined for sensitivity in the

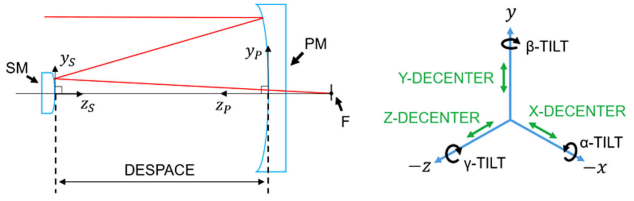

Fig. 2. Coordinate system for tolerance analysis (same abbreviations as in Fig. 1).

Table 1. Optical Design Parameters of the TRT Kit

		Newtonian	Cassegrain	Gregorian
Primary mirror	Aperture (mm)		150	
	Focal ratio		F/4	
	Surface type		Paraboloid	
Secondary mirror	Aperture (mm)	50	50	50
	Surface type	Flat	Hyperboloid	Ellipsoid
	Conic constant	—	−2.778	−0.458
Effective focal length (mm)		600	2400	3115
FOV[a] (with the 22.2 × 14.8 mm sensor) (′)		127.2 × 84.8	31.8 × 21.2	24.5 × 16.3

[a]Field of view.

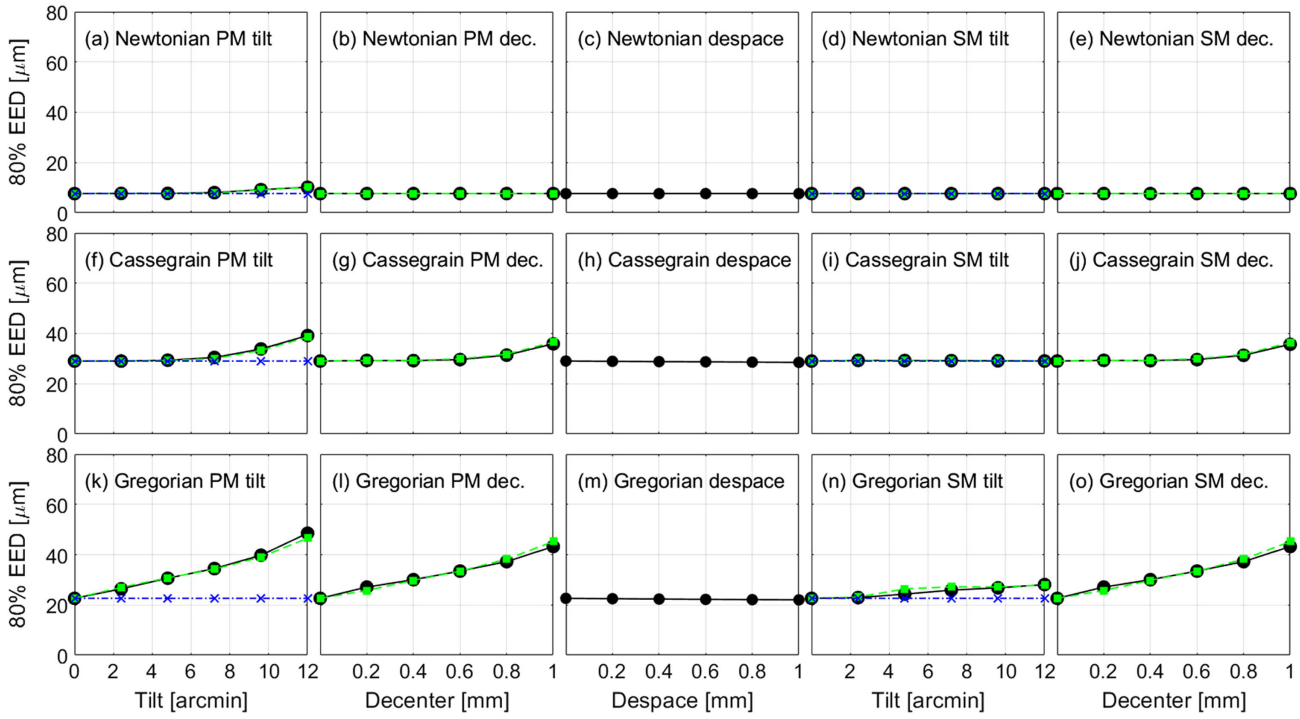

Fig. 3. Sensitivity analysis of Newtonian (top), Cassegrain (middle), and Gregorian (bottom) systems: (a), (d), (f), (i), (k), (n) α- (circle), β- (square), and γ- (cross) tilts; (b), (e), (g), (j), (l), (o) x- (circle) and y- (square) decenters; and (c), (h), (m) despace.

Newtonian, Cassegrain, and Gregorian telescope configurations. The criterion of the analysis is 80% encircled energy diameter (EED) for the 550 nm wavelength, and the focus is set as the compensator. Figure 3 shows sensitivity analysis results for the image center. 80% EED is displayed for each of the perturbed system parameters across all three telescope configurations. Calculated sensitivities for negative perturbations are symmetric to the positive cases.

The Newtonian secondary mirror is a simple flat mirror used to fold the optical path and does not affect optical performance. Figure 3 shows the constant 80% EED curves across decenters of the primary and secondary mirrors, tilts of the secondary mirror, and despace. Despace is not critical to optical performance for any of the three systems. Decenters of the primary and secondary mirrors have the same trends because they are coupled directly to each other. α- and β-tilts of the primary mirror are the most sensitive parameters for all three systems.

We performed Monte Carlo simulations as a statistical tolerance analysis to examine the effects of all errors simultaneously [9]. Monte Carlo simulation is performed for α- and β-tilts, x- and y-decenters, despace, and surface irregularity. The simulation is evaluated with 5000 trials at the 550 nm reference wavelength. The focus is set as the compensator to recover performance. The performance criterion is 12 μm for 80% EED, which is based on the Nyquist sampling requirement for a sensor with 6 μm pixels.

Table 2 lists the final tolerance ranges of three TRT configurations from the Monte Carlo simulation. The Gregorian is the most sensitive of the three systems analyzed. Overall tolerance ranges are acceptable and are within general fabrication and alignment errors. Alignment accuracy of the TRT kit will be discussed in Section 3.

Table 2. Tolerance Limits of Newtonian, Cassegrain, and Gregorian from the Monte Carlo Simulations

Parameter		Newtonian	Cassegrain	Gregorian
α-, β-Tilt	PM	±23′	±4′	±2.5′
	SM	±32′	±10′	±5′
x-, y-Decenter		±1 mm	±0.6 mm	±0.5 mm
Despace		±3 mm	±1 mm	±0.7 mm
Surf. irregularity		±2.5λ	±0.50λ	±0.35λ
Focus[a]		±20 mm		

[a]The focus is set as the compensator.

C. Optomechanical Design of TRT

The TRT kit is a modularized and portable system, enabling easy assembly of each type of telescope and adaptable optical test setup. The total dimensions are 610 mm (L) ×158 mm (W) ×188 mm (H), and the total weight is around 2 kg. The length extends to 970 mm in the Gregorian configuration. Illustrations for the Newtonian and Gregorian configurations are displayed in Fig. 4. The mounting base module contains the array of holes and taps like an optical table, so the TRT kit becomes transformable, and the equally spaced holes can be used for measuring distances such as focal length and despace. A precision linear stage is used for fine focusing with an accuracy of >10 μm, and 2-inch (50.8 mm) camera adapters are found near the two focal points. Red parts indicate optical mirrors.

Static analysis of the TRT kit was accomplished with SolidWorks (Dassault Systems) mechanical design software.

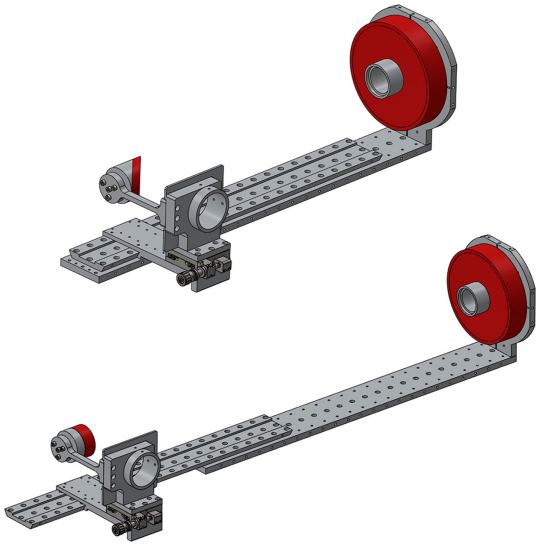

Fig. 4. 3D optomechanical modeling of the TRT kit. Newtonian (top) and Gregorian (bottom) systems are shown.

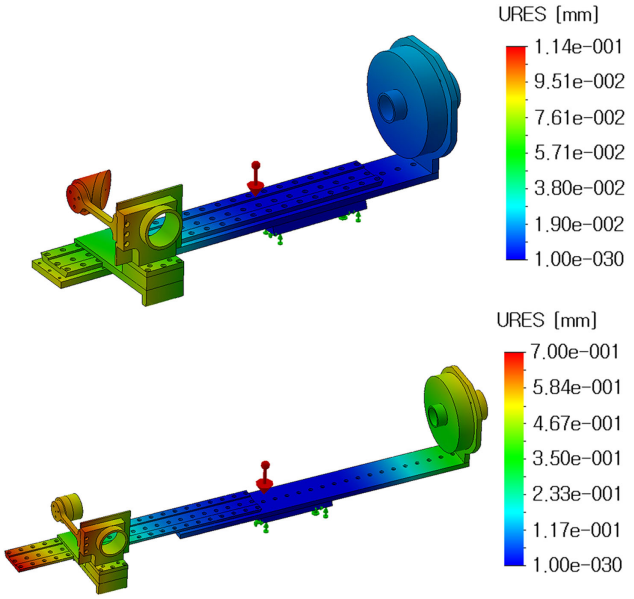

Fig. 5. Static analysis results of the compact mode (top) and extended mode (bottom). The red arrows represent gravity, and fixed (reference) positions are indicated with green arrows.

Optomechanical structures are made of aluminum alloy (Al6061-T6). The boundary condition used in the simulation fixes the bottom of the dovetail (green arrows in Fig. 5) in place, allowing other parts to move relative to this static mount.

The maximum mechanical deformations of optomechanical structures due to their weight are 0.11 mm and 0.7 mm for the compact (Newtonian, Cassegrain) and extended (Gregorian) configurations (Fig. 5), respectively. Based on tolerance analysis results, the mechanical deformations are not critical to optical performance.

3. TRT MANUFACTURING, ASSEMBLY, AND ALIGNMENT

A. Aluminum Mirror Fabrication

The primary mirror is made of aluminum alloy (Al6061-T6) with protected aluminum coated on the mirror surface. The aluminum mirrors have advantages over other substrates in handling and thermal stability, characteristics required for the portability of the system [10]. The TRT primary mirrors are easy to replace with mirrors of a different aperture size, surface type, and material. Fabrication processes of aluminum mirrors are as follows: pre-fabrication, stress relieving and aging, single-point diamond turning (SPDT), and protective coating. The entrance pupil diameter of the primary mirror is 150 mm, and it has an F-number of four (see Table 1).

The SPDT (Freeform 700A; Precitech) process produces a high-quality surface figure on the primary mirror. We employ a compensation strategy [11] to minimize low-frequency error (LFE) [12] and mid-frequency error (MFE) of the mirror surface.

We used the Ultrahigh Accurate 3D Profilometer (UA3P, Panasonic Corp.) to mechanically measure the mirror surface shape error using contact profilometry instead of optically measuring the errors [13–17].

Figure 6 represents surface measurement results of the fabricated aluminum primary mirror. The surface figure error of the mirror is 0.067 μm root mean square (RMS) and 1.84 μm peak to valley (PV). The average surface roughness (Ra) is 4.8 nm as measured with the WYKO NT2000 vertical scanning and phase-shifting interference microscope.

The primary and secondary mirrors are aluminum coated with >95% reflectivity, so the total throughput of the two-mirror telescopes is about 90.3% for all three configurations.

B. Assembly Method

The TRT kit has three main modules: a primary mirror module, secondary mirror module, and mounting base module. The modules are designed for interchangeability. The total number of optical and optomechanical components is 13. Screws and pins maintain the optical alignment. Because the modules are completely independent of one another, students may assemble each module separately and then cooperate to construct the final version of the TRT kit.

Figure 7 illustrates the assembly method of each module. (a) The mounting base module consists of four mechanical parts,

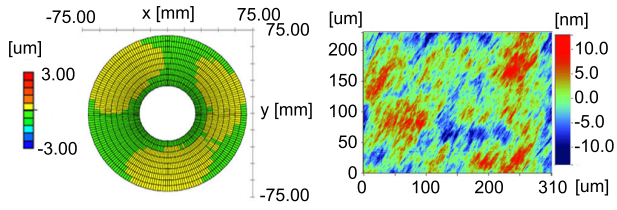

Fig. 6. Surface measurement results of the primary mirror. The overall surface shape is measured with the UA3P (left). The surface micro-roughness is measured with NT2000 (right).

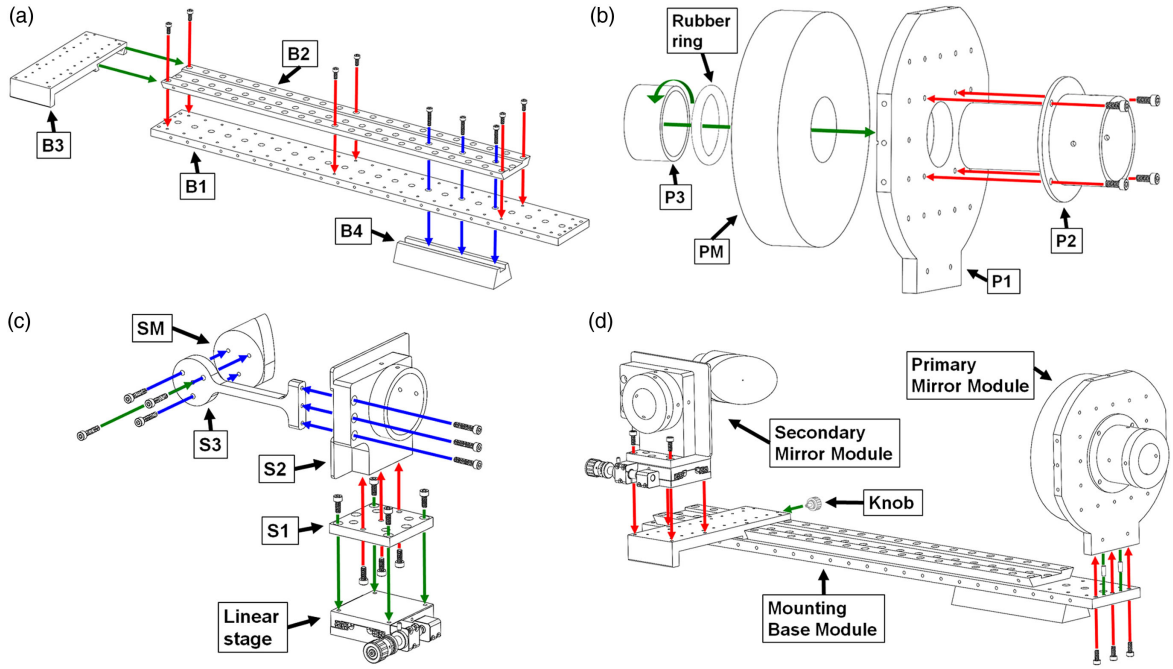

Fig. 7. The TRT assembly, including (a) mounting base module, (b) primary mirror module, (c) secondary mirror module, and (d) all three modules assembled in the final TRT kit configuration. Colored arrows indicate the screw and pin attachment points in the assembly process.

labeled B1 to B4, which support the primary and secondary mirror modules. The TRT kit mounts onto commercial telescope mounts, due to a universal dovetail adapter (B4) attached to the base. (b) The primary mirror is mounted to P1 by threading P3 to P2, and a rubber ring is inserted between P3 and the primary mirror to protect the reflective mirror surface. (c) The tip and tilt of the secondary mirror are adjusted with screws attached to the mirror through S3 and spaced 120° apart for three-point alignment. The linear stage for precise mirror transition is attached to S1, S1 is attached to S2, and S2 is attached to S3, the secondary mirror mount. The linear stage is then attached to B3 on the mounting base for precise positioning of the secondary mirror relative to the primary mirror. (d) The primary mirror module is fastened to the mounting base module with pins connecting P1 to B1. This mount configuration guarantees that the primary mirror support is attached perpendicular to the optical axis, drastically improving the simplicity of the design because only the secondary mirror must be aligned to the fixed primary mirror.

The primary mirror is aligned within $\pm 1.2'$ tolerance, which is measured by using coordinate measurement machines (CMMs), due to the pins between P1 and B1. The secondary mirror is replaced by other types using screws for S3 and the secondary mirror. The mounting base module needs to be reassembled for the Gregorian system (see bottom panel in Fig. 4).

C. Optical Alignment Process

Shack–Hartmann wave-front sensors and CMMs are commonly used for optical alignment [18]. Three-point laser alignment (TPLA) is another common practice used to align optics. TPLA uses three mounted lasers aligned parallel to the optical axis of the primary mirror.

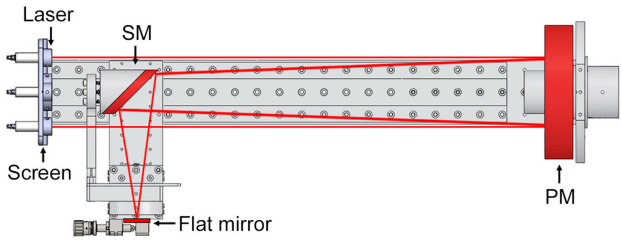

Fig. 8. Layouts of TPLA for the Newtonian telescope. This method can be adapted to the other types of telescopes (same abbreviations as in Fig. 1).

The laser mount contains a screen with holes at points optically conjugate to the sources. A flat mirror is placed at the focal plane of the optical system. First, the laser sources are emitted at the screen. Then, the beams reflect off of the primary mirror and converge towards the secondary mirror. For the Newtonian design, the flat secondary mirror then folds the optical path. Finally, the beams reflect off the flat at the focal point and return through the optical system to the screen. The laser sources reflect back through the optical system to the conjugate points of the sources only when all optical components are well aligned (see Fig. 8).

Figure 9 shows pictures of the TPLA alignment process. There are 3 mm diameter alignment holes at the conjugate points of the laser sources [panel (a) in Fig. 9] that are used for fine alignments. We measure coincidence of the laser point and the hole by eye within 0.5 mm uncertainty, which corresponds to $0.71'$, $0.18'$, and $0.14'$ tilt errors of the secondary mirror in Newtonian, Cassegrain, and Gregorian, respectively. These

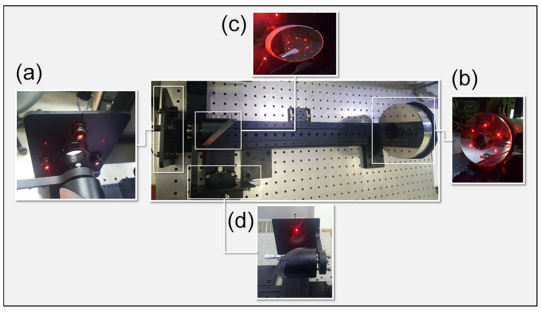

Fig. 9. The TRT kit alignment with TPLA method. (Center) Laser mount attached to the TRT kit. (a) Lasers come from the source (b) and are reflected by the primary mirror, (c) secondary mirror, (d) and flat mirror. After traveling back through the system, (a) the beams reach the screen.

alignment accuracies are acceptable by comparing to tolerances of the telescopes (Table 2).

4. TRT BAFFLE AND STRAY LIGHT CONTROL

Stray light analysis and effective baffle design are necessary to suppress unwanted light that degrades the image. Stray light is extraneous, unwanted light that is detected by the sensor reflection from mechanical structures or scattering from optical components. Stray light presents itself as noise in the image, reducing the signal-to-noise ratio (SNR).

The baffle design of on-axis reflective optical systems, such as Cassegrain and Ritchey–Chretien telescopes, is a well-defined process described by mathematical models. An iterative method is needed to design proper baffle systems [19–21].

For this portable optical device, stray light suppression is critical and even more important than it is for instruments operated indoors, as there are more potential sources of stray light when imaging outdoors. Baffle structures are easy to assemble with screws and T-mounts. Figure 10 demonstrates baffle structures suitable for all three optical configurations, though only the Newtonian configuration is shown. The plate baffles behind the primary and secondary mirrors are designed to effectively suppress critical stray light paths that directly illuminate the detector. These critical ray paths are of particular importance for the folded Newtonian system, which is susceptible to more potential sources of stray light as a result of the folded design.

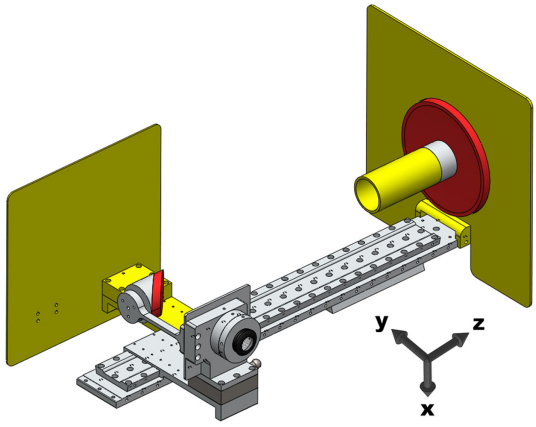

Fig. 10. The TRT kit with baffle structures. Yellow colors represent the baffles of the telescope.

Stray light analysis was completed with LightTools software (Synopsys Inc.). In the simulation, a 6500 K black body source was used to illuminate the optical system, approximating the spectral distribution of daylight. Assuming ideal diffusive surfaces, baffles and optomechanical structures scatter light with 1% and 5% Lambertian reflectance, respectively. Incidence angles of simulated stray light paths span 0°–180° for all systems. The amount of stray light suppression can be defined with the point source transmittance (PST):

$$\mathrm{PST}(\theta, \lambda_0) = \frac{L_\mathrm{D}(\theta, \lambda_0)}{L_\mathrm{A}(\theta, \lambda_0)}, \tag{1}$$

where $L_\mathrm{D}(\theta, \lambda_0)$ is spectral radiance on the detector, and $L_\mathrm{A}(\theta, \lambda_0)$ is spectral radiance on the entrance aperture. The PST represents how much stray light can be suppressed by the baffle structure as a function of incidence angle. Figure 11 presents results from stray light analysis for the TRT kit. Blue dots represent the PST with baffles, and red dots indicate the PST without baffles. The incident angles of 0°, 90°, and 180° indicate the incident light along $+z$, $-y$, and $-z$ direction, respectively (see Fig. 10 for the coordinate system).

Baffles suppress 75%–95% of stray light from all incidence angles (0° to 180°). The PST reaches a minimum of around 10^{-8} with baffles. Note that some of the sharp drops in PST near the 20° to 90° incidence angles for the Gregorian system are a result of under-sampling.

Compared to the other systems, the detector is most exposed to stray light without the baffle in the Newtonian system. Incoming stray light from specific angles (95°–118°, and around 170°) causes substantial degradation of image quality without the use of baffles. Suppression of stray light for incidence angles between 40° and 180° is particularly significant for the Newtonian system with the addition of baffles; 90% to 99.99% of stray light is suppressed in this region.

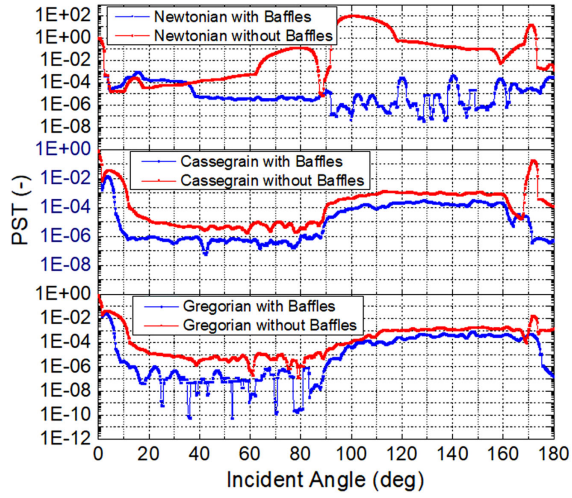

Fig. 11. Stray light analysis results of (a) Newtonian, (b) Cassegrain, and (c) Gregorian systems. Blue dots represent the PST with baffles, and red dots indicate the PST without baffles.

5. TRT SYSTEM PERFORMANCE AND APPLICATION

A. System Performance

The optical performance of the TRT kit was evaluated with three optical tests: observations of field images, point source tests, and night sky observations. Figure 12 includes pictures taken with the (a) Newtonian, (b) Cassegrain, and (c) Gregorian telescopes. These three pictures clearly indicate the difference in field of view (FOV) of the three configurations (see Table 1). The picture captured with the Gregorian telescope also shows the optically reversed image. The focal length can be derived from FOV of the observed image by calculating the plate scale.

Point source tests were also performed using the Newtonian configuration at the on-axis. Figure 13 shows the point source image with 23.8 μm 80% EED, corresponding to ∼3.7 pixels on a binned APS-C sensor. This is an appropriate spot size for scientific measurements because the Nyquist sampling theorem is satisfied, thereby avoiding under-sampling.

Fig. 12. TRT kit field test pictures. The pictures were captured with the (a) Newtonian, (b) Cassegrain, and (c) Gregorian telescopes, respectively. Each telescope has a different FOV, and the picture with the Gregorian telescope is reversed.

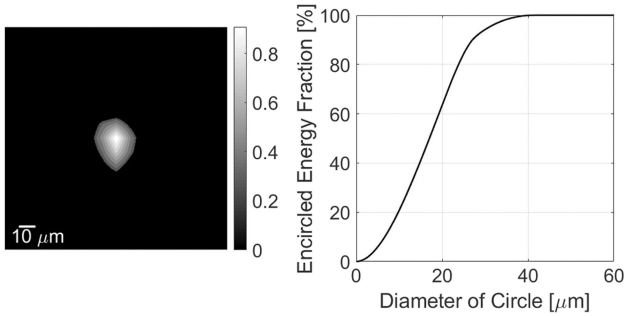

Fig. 13. Point source image (left) and EED (right).

Fig. 14. M27 nebula with stars that were observed using the Newtonian telescope.

Figure 14 depicts the Messier 27 (M27) nebula captured using the Newtonian TRT kit configuration. The observation demonstrates great optical performance, capable of imaging detailed structures of the extended source and the fine circular shapes of stars across the field.

B. Application to Spectroscopy

Since the TRT kit is modularized, it transforms to the spectrometer by installing the spectrometer module, which consists of a grating, a slit, and a light source. Figure 15 includes the main TRT kit, the baffles, and the spectrometer module to configure the Ebert–Fastie spectrometer.

A grating with 300 (grooves/mm) groove density and 4.3° blaze angle, and a neon lamp were installed for the spectrum illustrated in Fig. 16. At the position of the neon lamp, we can also place the focal plane of another telescope system to see the spectrum of distant targets. The commercial digital camera was installed for taking images. After the wavelength calibration, we clearly identified spectrum lines of the lamp in the wavelength range of 510 nm to 720 nm.

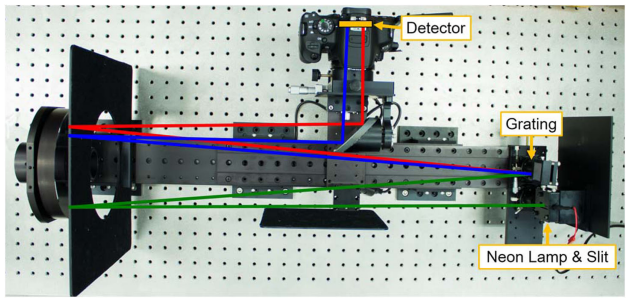

Fig. 15. Spectrometer module with the TRT kit.

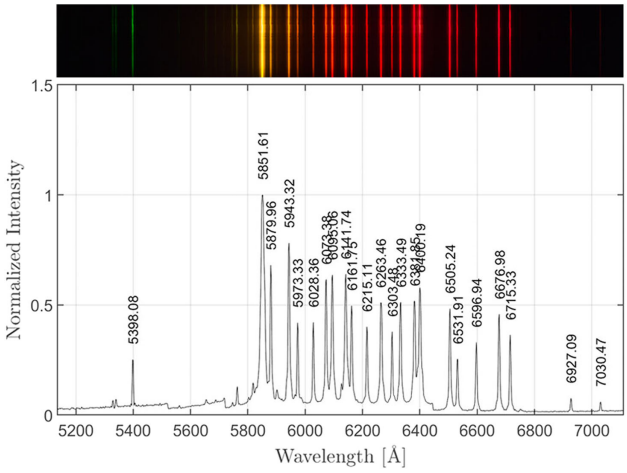

Fig. 16. Neon spectrum images from the TRT kit and the spectrometer module.

6. DISCUSSION AND SUMMARY

We developed the TRT kit to transform into the Newtonian, Cassegrain, and Gregorian telescopes, as well as the Ebert–Fastie spectrometer. The modular structure of the TRT kit maximizes versatility for various optical tests. Students need to replace only the secondary mirror to switch to other types of telescopes or optical systems.

The maximum optomechanical deformations by self-weight are 0.11 mm for Newtonian and Cassegrain configurations, and 0.7 mm for the Gregorian design. Even though these deformations may degrade the optical performance, the errors are acceptable by comparing to Monte Carlo simulation results.

Optimized baffle structures are designed for stray light suppression. They suppressed stray light from 10^{-1} to 10^{-8} PST across all angles of incidence.

The aluminum parabolic primary mirror was fabricated with SPDT. Surface errors on the primary mirror are $\leq\lambda/8$ RMS and, the average surface roughness is 4.8 nm. The mirrors are made of aluminum to prevent imaging quality degradation by nonuniform thermal expansion or contraction.

The TRT kit has a simple optical alignment procedure that requires only secondary mirrors to be aligned. The TPLA module makes optical alignment nearly effortless.

Point source measurement resulted in a 23.8 μm 80% EED. When observing the night sky, we were able to distinguish the fine structures of the M27 nebular. The TRT kit is useful not only for optical experiments but also as an astronomical telescope.

The TRT kit is a versatile, portable telescope and optical test system. It can be utilized for many optical experiments involving spectroscopy, Gaussian theory, and Fourier optics, and for developing an AO system by using the different types of telescope configurations such as Gregorian and Cassegrain, which create unique conjugate planes requiring different deformable mirror and wavefront sensor configurations. The compact size and portable design of the TRT kit enable its use in many different environments.

The TRT kit transformable design concept has obtained a domestic patent from the Korean Intellectual Property Office (application number KR10-2015-0153977) but the commercialization has not yet been processed. Estimated fabrication cost of optomechanical parts is about 600–1000 US dollars, which is probably affordable for high schools and universities. The TRT kit is suitable for both educational purposes and scientific research. We would like to widely distribute the transformable telescope kit to students, researchers, and others who are interested in using the kit.

Funding. Creative Convergence Research Project in the National Research Council of Science and Technology (CAP-15-01-KBSI).

Acknowledgment. This work was a collaborative research work with the Wyant College of Optical Sciences. This research was made possible in part by the Technology Research Initiative Fund Optics/Imaging Program at the University of Arizona.

Disclosures. The authors declare no conflicts of interest.

REFERENCES

1. P. Jiang, H. Yang, and S. Mao, "Design optical antenna and fiber coupling system based on the vector theory of reflection and refraction," Opt. Express **23**, 26104–26112 (2015).
2. S. V. Gavoronski and V. A. Zverev, "Versions of a mirror-objective composite based on an optical system of Gregory and Cassegrain objectives," J. Opt. Technol. **79**, 84–87 (2012).
3. A. Goncharov, M. Owner-Petersen, T. Andersen, J. Beckers, and N. Devaney, "Adaptive optics for the Euro50: design and performance," Proc. SPIE **4840**, 36–46 (2003).
4. M. Johns, C. Hull, G. Muller, B. Irarrazaval, A. Bouchez, T. Chylek, C. Smith, A. Wadhavkar, B. Bigelow, S. Gunnels, B. McLeod, and C. Buleri, "Design of the Giant Magellan Telescope," Proc. SPIE **9145**, 91451F (2014).
5. M. Akio and S. Takamasa, "Telescope commonly used for Cassegrainian and Newtonian systems," Publication number JPH1039233A (1998).
6. W. Kazuaki, "Reflecting telescope," Publication number JP2008309932A (2008).
7. A. Sarayotis, "Astronomical telescope with rotary closing blade," Publication number FR2923303A1 (2009).
8. L. C. N. Scaduto, J. Sasian, M. A. Stefani, and J. C. de Castro Neto, "Two-mirror telescope design with third-order coma insensitive to decenter misalignment," Opt. Express **21**, 6851–6865 (2013).
9. W. Park, S. Chang, J. H. Lim, S. Lee, H. Ahn, Y. Kim, S. Kim, A. Hammar, B. Jeong, G. H. Kim, H. Lee, D. W. Kim, and S. Pak, "Development of linear astigmatism free—three mirror system (LAF-TMS)," Publ. Astron. Soc. Pac. **132**, 044504 (2020).
10. T. Hadjimichael, D. Content, and C. Frohlich, "Athermal lightweight aluminum mirrors and structures," Proc. SPIE **4849**, 396–406 (2002).
11. X. Zhang, Z. Zeng, X. Liu, and F. Fang, "Compensation strategy for machining optical freeform surfaces by the combined on- and off-machine measurement," Opt. Express **23**, 24800–24810 (2015).
12. S. Kim, S. Chang, S. Pak, K. J. Lee, B. Jeong, G.-J. Lee, G. H. Kim, S. K. Shin, and S. M. Yoo, "Fabrication of electroless nickel plated aluminum freeform mirror for an infrared off-axis telescope," Appl. Opt. **54**, 10137–10144 (2015).
13. N. I. Chkhalo, I. V. Malyshev, A. E. Pestov, V. N. Polkovnikov, N. N. Salashchenko, M. N. Toropov, and A. A. Soloviev, "Problems in the application of a null lens for precise measurements of aspheric mirrors," Appl. Opt. **55**, 619–625 (2016).
14. J. C. Wyant and V. P. Bennett, "Using computer generated holograms to test aspheric wavefronts," Appl. Opt. **11**, 2833–2839 (1972).
15. X. Li, L. P. Zhao, Z. P. Fang, A. Asundi, and X. M. Yin, "Surface measurement with Shack-Hartmann wavefront sensing technology," Proc. SPIE **7155**, 715515 (2008).
16. J. Yu, F. Fang, and Z. Qiu, "Aberrations measurement of freeform spectacle lenses based on Hartmann wavefront technology," Appl. Opt. **54**, 986–994 (2015).
17. A. Lylova, G. Kalenkov, J. Sheldakova, S. Kalenkov, A. Kudryashov, and A. Shtanko, "Measurement of parabolic mirrors aberrations in hyperspectral microscope," Proc. SPIE **9641**, 96410N (2015).
18. K.-H. Wu, C.-C. Lie, Y.-C. Lin, C.-Y. Chan, T.-M. Huang, and M.-Y. Hsu, "Assembly aligning and measuring of a reflective telescope primary mirror," Proc. SPIE **9947**, 99470X (2016).
19. C.-F. Ho and S.-T. Chang, "Baffle design for a Cassegrain telescope," Proc. SPIE **7506**, 75061S (2009).
20. M. S. Kumar, C. S. Narayanamurthy, and A. S. K. Kumar, "Iterative method of baffle design for modified Ritchey-Chretien telescope," Appl. Opt. **52**, 1240–1247 (2013).
21. N. Song, Z. Yin, and F. Hu, "Baffles design for an axial two-mirror telescope," Opt. Eng. **41**, 2353–2356 (2002).